scientific reports

Check for updates

OPEN

Three-dimensional characterization of sex differences in abdominal aortic aneurysm progression via vascular deformation mapping

Drew J. Braet[1]✉, Timothy J. Baker[2], Luciano Delbono[1], Gregory Spahlinger[2], Nathan Graham[3], Akul Arora[3], C. Alberto Figueroa[1,4], Jonathan L. Eliason[1] & Nicholas S. Burris[2]

Although abdominal aortic aneurysms (AAA) are more common in men, women are at greater risk for AAA growth/rupture. Vascular deformation mapping (VDM) utilizes deformable image registration to qualify and quantify 3D-AAA growth using computed tomography angiograms (CTA). In this study we leveraged VDM to investigate sex differences in AAA growth patterns. Patients with infra-renal AAA and ≥ 2 CTA were identified. Males and females were matched for age, hypertension, and smoking history. Patient characteristics, maximum diameter (Dmax), and AAA volume were obtained. CTA images were segmented, and VDM was conducted to quantify 3D AAA growth rate per year (GR, cm/year). Statistical shape modeling was utilized to compute mean aneurysm shapes and 3D GR. Average GR was evaluated at specific regions of the aortic surface for males and females. Seventeen males and 17 females were matched. At the individual level, there were no sex differences in changes in Dmax or AAA volume. However, females had larger GR across the anterior and right lateral AAA (1.33 vs 0.89 and 1.56 vs 0.74 cm/year, respectively), despite no difference in posterior or left lateral AAA GR. Despite comparable changes in Dmax, AAA volume, and GR magnitude, women demonstrated a more eccentric, anterior-predominant, AAA growth pattern.

Keywords Aortic aneurysm, Sex characteristics, Aortic diseases

Abdominal aortic aneurysm (AAA) rupture potential increases with increasing maximum aortic diameter (Dmax) and carries a high risk of morbidity and mortality[1–7]. Thus, surgical repair of AAA is generally reserved for males with a Dmax of ≥ 5.5 cm, females with a Dmax of ≥ 5.0 cm, and rapidly growing AAAs[5,8,9]. However, Dmax does not account for the complexities of AAA morphology and may be inadequate for evaluating AAA progression and rupture[10–13]. Although AAA volume measurements are promising for assessing AAA growth and rupture risk, little is known about AAA volume growth patterns and their relationship to disease progression[14–20].

While AAAs are more common in men, women may be at greater risk for AAA growth and rupture[21–27]. The mechanisms of sex differences in AAA growth and rupture are likely multifactorial[28]. However, there are sex differences in aneurysm morphology, with females having greater neck angulation, shorter aortic neck length, and higher anatomic severity grade[29,30]. Moreover, saccular aneurysms, which are composed of a localized area of growth, are more common in females than in males[31]. Compared to fusiform aneurysms, which have concentric areas of growth, saccular aneurysms are thought to have a greater risk of rupture and are thus often treated at smaller diameters[32,33].

Vascular deformation mapping (VDM) is a novel technique that utilizes deformable image registration to quantify three-dimensional (3D) changes in aortic growth using routine clinical computed tomography angiogram (CTA) images. VDM has been used to assess growth in both thoracic aortic aneurysms and AAAs, with prior works showing significant discrepancies in growth assessment between Dmax and 3D assessment of growth by VDM[34–38]. These findings have been supported by another group who used a similar 3D growth

[1]Section of Vascular Surgery, Department of Surgery, University of Michigan, 1500 E Medical Center Drive, Ann Arbor, MI 48109, USA. [2]Department of Radiology, University of Michigan, Ann Arbor, MI, USA. [3]Department of Surgery, University of Michigan, Ann Arbor, MI, USA. [4]Department of Biomedical Engineering, University of Michigan, Ann Arbor, MI, USA. ✉email: djbraet@med.umich.edu

mapping technique[39]. In this study, we aimed to leverage VDM to investigate sex differences in AAA growth. Given the described higher rupture risks and more hostile anatomy, we hypothesize that females will display greater degrees of focal/eccentric growth than males.

Results

Patient demographics

Thirty-four patients were included (Supplementary Fig. 1). Seventeen males and 17 females were matched for age, smoking history, and history of hypertension. The average age was 72.3 ± 7.3 years, and 91.2% of the patients were Caucasian. Most patients (88.2%) were current/former smokers, 76.5% had hypertension, and 20.6% had diabetes. There were no sex differences observed for race or diabetes status. Four (11.8%) patients had symptomatic AAAs, and 9 (26.5%) underwent AAA repair. The rates of symptomatic AAA and repair did not differ between the sexes (Table 1).

Diameter, volume, and tortuosity

The average baseline Dmax and average AAA volume were 4.7 ± 0.6 cm and 97.7 ± 58.5 cm^3, respectively. There was a trend toward greater baseline Dmax (4.9 ± 0.6 vs 4.5 ± 0.6 cm, $p = 0.055$) and greater baseline AAA volume in males than in females (118.7 ± 69.9 vs 76.6 ± 35.0 cm^3, $p = 0.034$). The average baseline intraluminal thrombus (ILT) volume was 41.1 ± 36.2 cm^3, with no sex difference (48.6 ± 37.3 vs 33.7 ± 34.6 cm^3, $p = 0.237$). The average increase in Dmax between CT scans was 0.041 ± 0.045 cm/month, and the increase in AAA volume was 1.55 ± 2.11cm^3/month. The average change in ILT volume was 0.58 ± 1.80 cm^3/year. There was no difference in the absolute change in Dmax (0.034 ± 0.023 vs 0.0488 ± 0.059 cm/month, $p = 0.400$), change in AAA volume (1.69 ± 1.69 vs 1.40 ± 2.50 cm^3/month, $p = 0.700$), or change in ILT volume (0.78 ± 1.25 vs 0.37 ± 2.25 cm^3/month, $p = 0.510$) between males and females. The average time interval between CTAs was 13.5 ± 9.8 months (range 1.0–33.4 months) and did not differ between sexes. Only one patient had an interval between CTAs of 1 month, with all other patients having an interval between CTAs of over 3.5 months. There was no sex difference in tortuosity (Table 1).

Average neck Dmax at baseline was 3.04 ± 0.42 cm and average neck length at baseline was 2.97 ± 2.06 cm. Average alpha-angle was 18.42 ± 6.97° and average beta-angle was 28.86 ± 12.69° at baseline. There was no difference in the baseline neck Dmax, neck length, alpha angle, or beta angle at baseline between sexes. Average

	Cohort n = 34	Male n = 17	Female n = 17	P-value
Patient demographics				
Age (years)	72.32 ± 7.31	72.41 ± 7.53	72.24 ± 7.32	0.945
Race: caucasian	31 (91.2)	14 (82.4)	17 (100.0)	0.101
Smoking: current/former	30 (88.2)	15 (88.2)	15 (88.2)	1.000
Hypertension	26 (76.5)	13 (76.5)	13 (76.5)	1.000
Diabetes	7 (20.6)	5 (29.4)	2 (11.8)	0.203
Symptomatic	4 (11.8)	1 (5.9)	3 (17.7)	0.287
Repair	9 (26.5)	4 (23.5)	5 (29.4)	0.697
Aneurysm measurements				
Baseline maximum AAA Dmax (cm)	4.65 ± 0.60	4.85 ± 0.59	4.45 ± 0.56	0.055
Baseline AAA Volume (cm3)	97.65 ± 58.46	118.68 ± 69.89	76.62 ± 35.01	0.034
Baseline ILT Volume (cm^3)	41.12 ± 36.23	48.55 ± 37.34	33.68 ± 34.59	0.237
Change in diameter (cm/month)	0.041 ± 0.045	0.034 ± 0.023	0.048 ± 0.059	0.400
Change in AAA Volume (cm^3/month)	1.55 ± 2.11	1.69 ± 1.69	1.40 ± 2.50	0.700
Change in ILT volume (cm^3/month)	0.58 ± 1.80	0.78 ± 1.25	0.37 ± 2.25	0.510
Time Interval Between CTA (months)	13.50 ± 9.82	11.56 ± 8.94	15.43 ± 10.53	0.257
Tortuosity	0.08 ± 0.06	0.08 ± 0.05	0.08 ± 0.05	0.743
Neck measurements				
Baseline neck Dmax (cm)	3.04 ± 0.42	3.06 ± 0.44	3.03 ± 0.42	0.841
Baseline neck length (cm)	2.97 ± 2.06	3.51 ± 1.68	2.40 ± 2.32	0.126
Baseline alpha-angle (°)	18.42 ± 6.97	17.13 ± 7.57	20.03 ± 6.06	0.292
Baseline beta-angle (°)	28.86 ± 12.69	27.12 ± 13.80	31.03 ± 11.36	0.437
Change in neck Dmax (cm/month)	0.02 ± 0.07	0.01 ± 0.05	0.03 ± 0.09	0.424
Change in neck length (cm/month	-0.08 ± 0.28	-0.10 ± 0.29	-0.06 ± 0.29	0.683
Change in alpha-angle (°)	1.42 ± 7.09	2.49 ± 3.28	-0.06 ± 10.46	0.454
Change in beta-angle (°)	3.67 ± 4.31	2.58 ± 2.95	5.12 ± 5.50	0.188

Table 1. Patient demographics and diameter/volume measurements. Data are presented as n (%) for categorical variables and mean ± standard deviation (SD) for continuous variables. VDM, vascular deformation mapping; AAA, abdominal aortic aneurysm; ILT, intraluminal thrombus.

change in neck Dmax was 0.02 ± 0.07 cm/month and average change in neck length was − 0.08 ± 0.28 cm/month. Average change in alpha angle was 1.42 ± 7.09° and average change in beta angle was 3.67 ± 4.31°. There was no difference in the change of neck Dmax, neck length, or neck angle between sexes (Table 1).

3-Dimensional AAA growth patterns of males and females

There was a heterogeneous distribution of individual growth patterns, with minimal growth, focal/eccentric growth, and diffuse growth patterns observed in both male and female AAAs. Representative examples of growth patterns from matched pairs of male and female AAAs (4/17 matched pairs) are shown in Supplementary Fig. 2 (all 17 matched pairs are shown in Supplementary Fig. 3). In these examples, male AAAs demonstrate more diffuse growth and higher growth rates than their matched female counterparts, which display more focal/discrete growth patterns.

Sex-specific AAA growth patterns by statistical shape modeling

Figure 1 depicts the mean shapes and growth rate (GR) pooled for each patient sex group computed by statistical shape modeling (SSM) analysis of individual VDM results. One female growth map was excluded as an outlier from SSM analysis due to significant irregular growth and ILT deposition. The mean growth in males appears relatively circumferential, sparing only a small region of the posterior wall that abuts the lumbar spine, compatible with a diffuse growth profile and fusiform shape of the aneurysm. The mean growth in females demonstrated a more eccentric growth profile, skewed toward the anterior and right lateral wall, with two areas of significant anterior and lateral growth. Additionally, the mean growth profile in females demonstrated a greater degree of involvement of the aneurysm neck.

In terms of the mean growth derived from shape models, females had a greater overall GR (0.12 vs 0.09 cm/year, $p < 0.001$). Additionally, females had a greater percentage of AAA surface area with a GR > 0.1 cm/year (71.3% vs 41.0%, $p < 0.001$) and 0.2 cm/year (6.7% vs 0.0%, $p < 0.001$) than males, supporting more focal areas of growth.

Comparison of aneurysm shape by sex

Baseline differences in AAA regional size (i.e., distance from the centerline) are shown in Fig. 2 and Table 2. The baseline AAA regional size was greater in males across all AAA segments (anterior: 1.87 ± 0.60 vs 1.78 ± 0.69 cm, $p < 0.001$; right lateral: 1.80 ± 0.61 vs 1.64 ± 0.62 cm, $p < 0.001$; posterior: 1.76 ± 0.57 vs 1.40 ± 0.47 cm, $p < 0.001$; left lateral: 1.89 ± 0.60 vs 1.63 ± 0.59 cm, $p < 0.001$). Females had larger anterior aneurysm necks (1.41 ± 0.42 vs 1.61 ± 0.50 cm, $p < 0.001$), while males had larger posterior aneurysm necks (1.58 ± 0.60 vs 1.41 ± 0.36 cm, $p < 0.001$). There was no difference in the baseline aneurysm neck size between the right lateral (1.49 ± 0.53 vs 1.49 ± 0.42 cm, $p = 0.654$) and left lateral (1.52 ± 0.52 vs 1.53 ± 0.42 cm, $p = 0.372$) segments.

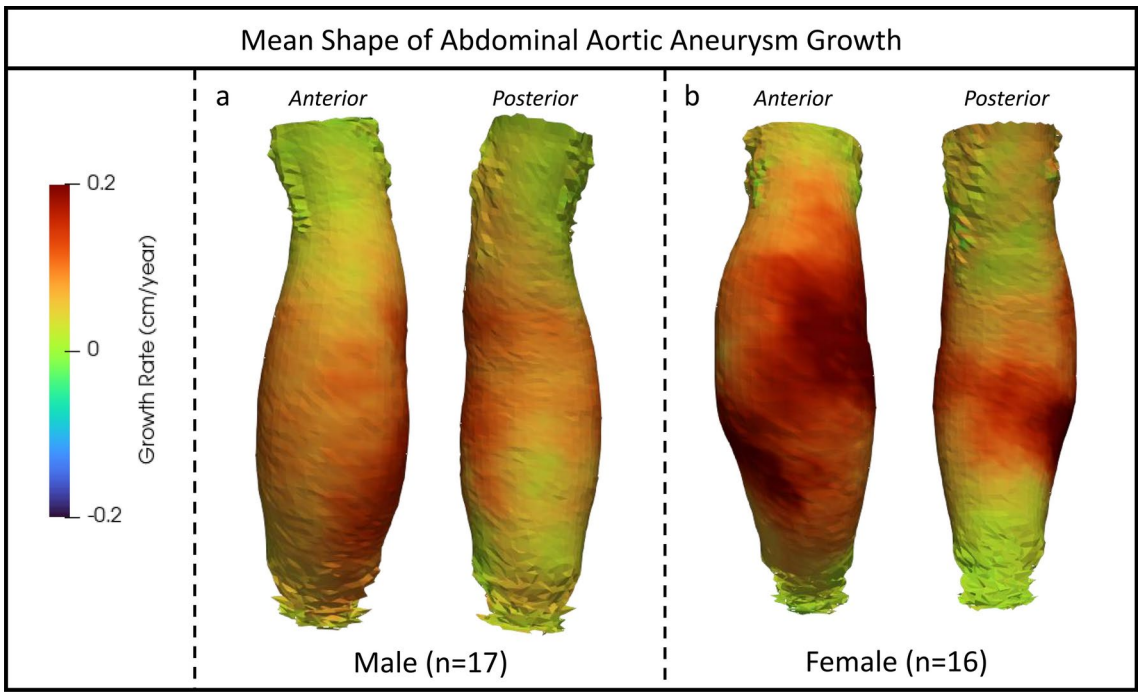

Fig. 1. Mean three-dimensional abdominal aortic aneurysm shapes and corresponding growth maps for males (**a**) and females (**b**) by statistical shape modeling. Growth is displayed using a colorized scale (Green = 0 cm/year, Red = 0.2 cm/year). Note: one female growth map was excluded because it included severe deviation in growth and was deemed an outlier.

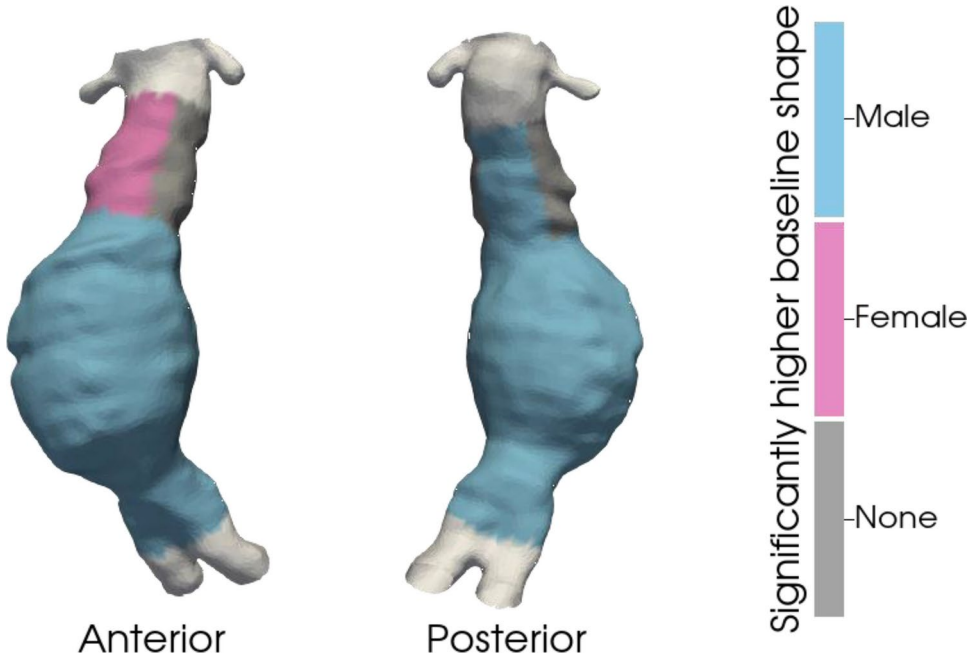

Fig. 2. Three-dimensional display of differences in baseline AAA size by aortic region between males and females overlying a sample aorta. Blue denotes a higher value in males. Pink displays a higher value in females. Grey denotes no difference.

	Anterior	Right Lateral	Posterior	Left Lateral
Baseline shape (cm)	Male versus Female (*p*-value)			
AAA	1.87 ± 0.60 vs 1.78 ± 0.69 ($p < 0.001$)	1.80 ± 0.61 vs 1.64 ± 0.62 ($p < 0.001$)	1.76 ± 0.57 vs 1.40 ± 0.47 ($p < 0.001$)	1.89 ± 0.60 vs 1.63 ± 0.59 ($p < 0.001$)
Aneurysm neck	1.41 ± 0.42 vs 1.61 ± 0.50 ($p < 0.001$)	1.49 ± 0.53 vs 1.49 ± 0.44 ($p = 0.654$)	1.58 ± 0.60 vs 1.41 ± 0.36 ($p < 0.001$)	1.52 ± 0.52 vs 1.53 ± 0.42 ($p = 0.372$)
Growth rate (cm/year)	Male vs Female (*p*-value)			
AAA	0.89 ± 1.21 vs 1.33 ± 2.01 ($p < 0.001$)	0.74 ± 0.86 vs 1.56 ± 3.66 ($p < 0.001$)	0.93 ± 1.27 vs 0.94 ± 1.92 ($p = 0.468$)	1.31 ± 1.77 vs 1.26 ± 1.88 ($p = 0.087$)
Aneurysm neck	0.45 ± 0.84 vs 0.95 ± 1.43 ($p < 0.001$)	0.43 ± 0.62 vs 0.67 ± 1.15 ($p < 0.001$)	1.09 ± 1.51 vs 0.59 ± 0.64 ($p < 0.001$)	0.83 ± 1.21 vs 0.84 ± 1.66 ($p = 0.655$)

Table 2. Sex differences in baseline shape and growth rate by aortic segment. AAA, abdominal aortic aneurysm.

Comparison of aneurysm growth by sex

Sex differences in AAA growth are shown in Fig. 3 and Table 2. Despite a larger baseline AAA size in males, females had greater GRs on the anterior (1.33 ± 2.01 vs 0.89 ± 1.21 cm/year, $p < 0.001$) and right lateral (1.56 ± 3.66 vs 0.74 ± 0.86 cm/year, $p < 0.001$) AAA surfaces. There was no sex difference in the GR at the posterior (0.93 ± 1.27 vs 0.94 ± 1.92 cm/year, $p = 0.468$) or left lateral (1.31 ± 1.77 vs 1.26 ± 1.88 cm/year, $p = 0.087$) AAA segments, supporting an eccentric growth profile in females. In the aneurysm neck, females had larger GRs on the anterior (0.95 ± 1.43 vs 0.45 ± 0.84 cm/year, $p < 0.001$) and right lateral (0.67 ± 1.15 vs 0.43 ± 0.62 cm/year, $p < 0.001$) surfaces, while males had larger GRs on the posterior surface (1.09 ± 1.51 vs 0.59 ± 0.64 cm/year, $p < 0.001$). There was no difference in the GR on the left lateral segment of the aneurysm neck (0.83 ± 1.21 vs 0.84 ± 1.66 cm/year, $p = 0.655$).

Comparison of aneurysm curvature by sex

Sex differences in AAA curvature are shown in Table 3. There was no difference in baseline AAA or aneurysm neck curvature at the anterior, right lateral, posterior, or left lateral segments between males and females ($p > 0.05$ for all).

Discussion

Our findings clearly demonstrate that VDM provides a nuanced assessment of 3D AAA growth, highlighting growth that may not be captured by standard Dmax and AAA volume measurements. AAAs exhibit a wide variety of 3D growth patterns, with some exhibiting little to no growth, others exhibiting focal growth, and others exhibiting diffuse growth. When matched for risk factors for AAA growth, females and males demonstrated sex-specific distributions of growth. Females demonstrated growth profiles that favored the anterior wall and resulted in eccentric growth with areas of focal growth and larger growth in the anterior aneurysm neck. On

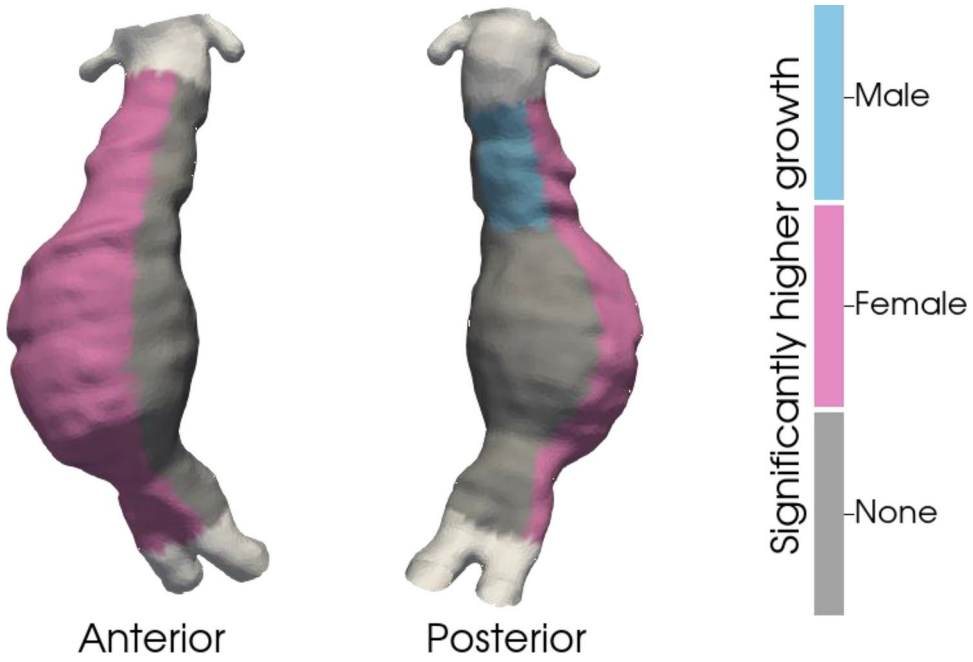

Fig. 3. Three-dimensional display of differences in growth rate by aortic region between males and females overlying a sample aorta. Blue denotes a higher value in males. Pink displays a higher value in females. Grey denotes no difference.

	Anterior	Right lateral	Posterior	Left lateral
Baseline curvature	Male versus Female (p-value)			
AAA	0.019 ± 0.004 versus 0.021 ± 0.005 ($p = 0.240$)	0.020 ± 0.004 versus 0.020 ± 0.004 ($p = 0.799$)	0.019 ± 0.005 versus 0.020 ± 0.005 ($p = 0.322$)	0.019 ± 0.005 versus 0.021 ± 0.005 ($p = 0.299$)
Aneurysm Neck	0.018 ± 0.007 versus 0.016 ± 0.006 ($p = 0.458$)	0.019 ± 0.007 versus 0.016 ± 0.006 ($p = 0.271$)	0.018 ± 0.007 versus 0.016 ± 0.006 ($p = 0.429$)	0.020 ± 0.007 versus 0.016 ± 0.007 ($p = 0.206$)

Table 3. Sex differences in curvature by aortic segment. AAA, abdominal aortic aneurysm.

the other hand, males demonstrated a more diffuse growth pattern involving greater aneurysm circumference, resulting in a more fusiform aneurysm shape. Analysis of 3D growth patterns by VDM provides novel and nuanced qualitative and quantitative information regarding reported sex differences in AAA progression.

Our study utilized SSM to compare the mean 3D growth shapes of AAAs between sexes, a technique that has been widely employed in a variety of diseases to identify anatomic differences between groups in a manner that helps overcome inter-individual variability that can obscure the detection of disease patterns[40–47]. Specifically, SSM employs geometric models that describe a collection of similar objects in a compact way, thus representing the average shape of many 3D objects as well as their variation in shape[40]. In brief, a principal component analysis is performed, which provides information about linearly independent components, thus describing the variation in the shape of the population and highlighting potential interactions between morphological characteristics of these different components[41]. SSM is an objective model that provides unique 3D shape information and, as our data support, is a promising tool for assessing differences in AAA growth/progression. A unique advantage of our implementation of SSM is that our statistical models included both shape information, as is required for standard SSM, as well as 3D growth data extracted from VDM, allowing for the depiction of the relationships between aneurysm shape and growth patterns in a manner not previously performed in AAA.

Although men are more susceptible to developing AAA, women are at greater risk for AAA growth and rupture[21–23]. The mechanism driving the increased risk of rupture in women is unclear and likely multifactorial, with some authors suggesting that it is a result of unfavorable biomechanical properties of the female aorta (decreased tensile strength in female aortas) and others suggesting sex differences in AAA anatomy[28–30,48]. When controlling for age and AAA size, sex differences in aortic neck length, diameter, and angulation have been described[29]. Other authors have shown sex differences in the anatomic severity grade, as well as the iliac artery diameter and length[30]. These findings are compatible with our observation that AAA growth is more eccentric and involves the aneurysm neck to a greater degree in women. These patterns of growth could predispose to the greater angulation and anatomic complexity observed in females.

While the majority of AAAs grow in a fusiform manner, approximately 6% demonstrate saccular growth[31]. Saccular aneurysms are thought to pose a greater rupture risk than their fusiform counterparts and thus are

often treated at small diameters[9,31–33,49]. Patients with saccular AAAs, both at large (> 5.5 cm) and small Dmax (< 4.5 cm), are more likely to have symptomatic/ruptured AAAs, and 42% of ruptured AAAs < 5.5 cm are saccular shaped[31,33]. Additionally, saccular aneurysms may be more common in females than in males[31]. In our study, although most patients had fusiform growth, males appeared to have more diffuse growth profiles, while females appeared to have more focal/eccentric growth patterns. The focal/eccentric growth patterns observed in females in this study, although not truly saccular, may provide insight into the sex differences observed in AAA rupture rates, which could be driven by differences in mean growth shapes. The VDM technique provides unique information about growth in three dimensions and appears to be a useful adjunct to explore sex differences in AAA progression.

Biomechanical studies of AAAs have supported the role of aneurysm shape and geometry in the risk of rupture, with aneurysm asymmetry being linked to greater aortic wall stress[13,50]. When matched for age, sex, and diameter, ruptured AAAs have been found to be less tortuous, with greater cross-sectional asymmetry in diameter, thus highlighting the superiority of AAA geometry over Dmax in predicting rupture risk[51]. Additionally, saccular aneurysms have greater wall stress than fusiform aneurysms, indicating that aneurysm shape influences wall stress and presumably rupture risk[52]. Moreover, greater curvature has been postulated to be an important surrogate for aortic wall stress and associated with both increased annual AAA growth and AAA rupture[53–55]. Although our analysis did not reveal differences in curvature or assess biomechanical stress between male and female AAAs, our results taken into context with these studies support the idea that differences in AAA anatomy and growth between men and women may contribute to the observed differences in rupture risk. However, future studies are needed to better define these differences and provide information regarding their underlying mechanisms.

This work has several key limitations. First, the VDM technique currently relies on clear delineation of the aortic wall separate from adjacent structures (e.g., bowel and inferior vena cava), which was not possible in some cases despite detailed manual correction of segmentations. Furthermore, the VDM technique was originally developed for the treatment of thoracic aortic aneurysms, a pathology that is significantly less prone to ILT formation. There were 6 patients in our cohort with extensive ILT in which registration and VDM analysis were considered unreliable; these patients were excluded due to misregistration at the boundary between the ILT and surrounding periaortic fat (Supplemental Fig. 1). Additionally, while VDM registration itself takes only 20–30 min to perform, the entire analysis workflow requires manual effort to review and edit aortic segmentations and perform quality assurance of the output and thus is currently more time-consuming than ideal for clinical practice. Technical development is ongoing to increase the automation of VDM and SSM analysis to address these challenges. In this analysis, we only included patients who had ≥ 0.1 cm increase in Dmax between CT scans. Given that the variability of AAA Dmax measurements from CTA is as high as 0.5 cm[56,57], our inclusion criteria may have introduced a potential bias to our study results. However, because VDM utilized 3D image data, rather than the 2D plane used for Dmax measurements there is higher accuracy and less variability in VDM derived growth. Additionally, VDM uses non-rigid image registration techniques that align CTA images with a precision of 0.5–1.0 mm, thus providing higher accuracy than manual Dmax measurements[58]. Although several studies support the notion that females have larger and faster growth than males at same AAA Dmax[21–27], this has not been demonstrated by other authors[59]. Thus, it is possible that by not matching our cohorts by AAA Dmax we biased our results. However, we felt that controlling for baseline Dmax could bias towards more advanced disease relative to body size and higher growth rates in females, thus limiting the potential to assess sex differences. In the present study we compared growth and shape across eight discreet segments of the aorta. Although using eight segments helps with the clinical interpretability of our results, it is possible that we did not capture more nuanced growth patterns occurring on a smaller scale. Also, our study did not assess aortic remodeling which could be present without significant geometric changes. Moreover, in this study we did not assess ILT shape or growth patterns which could play an important role in baseline shape and/or growth rate differences. Last, this study involved only a small cohort of largely Caucasian patients from a single center and thus may not be representative and/or generalizable to other populations. Studies on more diverse populations of AAA patients with larger sample sizes are needed to verify the preliminary observations of this study.

VDM yields important qualitative and quantitative information about AAA growth that is not discernable with current clinical techniques. When matched for common risk factors, females demonstrated a greater degree of focal/eccentric AAA growth along the anterior wall with greater involvement of the anterior aneurysm neck than males despite a lack of difference in the rate of growth according to standard diameter and volume measurements. These sex-specific patterns of AAA growth may contribute to the observed increased rupture risk and anatomic complexity in women, and the mechanisms underlying these distinct patterns should be further investigated.

Methods

Study population

Patients who were previously diagnosed with infrarenal AAA between 2010 and 2021 were identified using an institutional dataset and International Classification of Diseases (ICD) (ICD-10 and ICD-9) codes (Supplementary Table 1). Patients were included if they had native infrarenal AAAs, had ≥ 2 available abdominal aortic CTAs completed at least one month apart and prior to surgical repair, or had AAA interval growth (defined as > 0.1 cm between two CTA scans) according to clinical reports. Patients were excluded if they had suboptimal aortic enhancement, non-contrast CT scans, isolated thoracic aneurysms, poor imaging quality, or a lack of 2 CTAs completed at least one month apart prior to repair. General demographic information, past medical, smoking, and surgical history was collected by chart review. Males and females were matched for age, hypertension status, and smoking history. Patients were not matched for aneurysm size to avoid diluting known sex differences in aneurysm morphology. This study was reviewed and approved by the University of Michigan Medical School

Institutional Review Board, and a waiver of informed consent was granted. All methods were performed in accordance with the relevant guidelines and regulations.

Image segmentation

Digital Imaging and Communications in Medicine (DICOM) data for the CTA scans were exported and deidentified. Automated segmentations of the entire aorta, including the aortic blood volume (AAA lumen) and ILT, and its branches were completed using PRAEVAorta (Nurea, Bordeaux, France). Segmentations were manually confirmed for accuracy using 3D Slicer[33]. Segmentations started at the subdiaphragmatic abdominal aorta and ended at the iliac bifurcation and included the celiac artery, superior mesenteric artery, and bilateral renal arteries. The inferior mesenteric artery was not included. The AAA lumen and ILT segmentations were completed manually. All segmentations were reviewed by one investigator (D.B.) with over 4 years of image segmentation experience who was blinded to the patient's identity and sex.

Vascular deformation mapping

VDM analysis was performed using a previously reported workflow[34]. Briefly, VDM involves multistep image registration of aortic CTAs to generate a deformation field that is used to quantify localized aortic growth in a 3D fashion. The steps involved in VDM analysis include (1) segmentation of the abdominal aorta on CTAs acquired at two different time points, with the first considered the fixed image and the second considered the moving image; (2) image preprocessing, cropping, application of an edge sharpening filter, and dilation of aortic masks by 3 voxels to ensure inclusion of the wall; (3) rigid registration (Euler) to approximately align the two CTAs (Elastix, Utrecht, Netherlands)[60]; (4) alignment of the aortic centerline using a highly regularized multi-image, multi-metric deformable registration, which applies a penalty term to enforce rigid movement of voxels within the aortic segmentation while allowing deformation of the peri-aortic voxels optimized rigid aortic registration[61]; (5) multi-resolution, multimetric b-spline deformable image registration using mutual information with 10 mm grid spacing and a bending energy penalty of 20; (6) generation of a polygonal mesh of the aortic surface (100,000–400,000 surface elements) at baseline (fixed) geometry; (7) translation of mesh vertices of baseline mesh using the deformable image registration field calculated in Step 5; and (8) quantification of the degree of deformation in the direction normal/perpendicular to the surface of the aortic wall in centimeters, normalized by the time interval to yield normal deformation per years, which we refer to as growth rate (GR), visualized in Paraview (Kitware Inc., Clifton Park, NY, USA). A lack of aortic growth (GR = 0 cm/year) is depicted in green, whereas aortic growth (GR > 0 cm/year) is visualized in yellow and red, and compression (GR < 0 cm/year) is depicted in blue (Fig. 4). VDM outputs underwent a multi-step quality assurance (QA) protocol that included verification of the lack of segmentation errors and inspection of a dual-channel image created using a gradient magnitude filter to ensure accurate registration of the outer aortic wall. If a patient had multiple surveillance intervals (i.e., ≥ 3 CTAs), only the longest surveillance interval for each AAA that passed the QA assessments was included.

Definition of AAA centerlines, shape, curvature, and regions

Aortic centerlines were calculated from baseline segmentation meshes using the Vascular Modeling Toolkit (VMTK), and baseline shape was calculated by measuring the distance (cm) of the aneurysm surface at baseline from the aortic centerline[62]. Curvature was defined as the inverse of the radius of the circle that approximates the curve and measures the deviation of the curve from a straight line[63]. To allow for a reproducible assessment of differences in shape and GR, the aorta was divided into regions. First, longitudinal zones were defined by setting a value of 1 at the iliac bifurcation and then increasing by 1 for every 5% along the centerline toward the renal arteries (range 1–19). The AAA region was defined as longitudinal zones 1–14, and the aneurysm neck was defined as longitudinal zones 15–19. Lateral zones were defined by setting a value of 1 for points normal to the

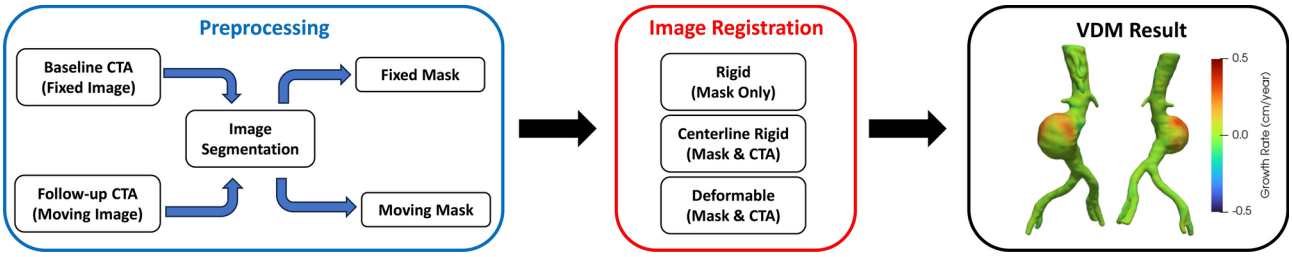

Fig. 4. Schematic overview of the steps in vascular deformation mapping (VDM) analysis. First, computed tomography angiography (CTA) scans at two time points (baseline and follow-up) undergo segmentation (blue box). Second, a multi-step registration of the two CTAs is performed including a rigid registration step to approximately align the two scans, followed by a highly regularized deformable registration with rigidity penalty to implicitly align the aortic centerlines ("centerline rigid"), and finally a b-spline deformable registration to align the outer wall of the aortas (red box). Lastly, a mesh of the abdominal aorta is created from the baseline CT mask and 3D deformation/growth metrics from the final deformable registration are plotted on the aortic surface. Growth is quantified as the degree of aortic expansion in the direction perpendicular (normal) to the aortic wall and normalized to interval to yield a growth rate in millimeters per year (black box) and displayed using a colorized scale (Green = 0 cm/year, Red = 0.5 cm/year).

plane of the iliac bifurcation and then increasing by 1 for every 30° circumferentially (range 1–12). Four lateral regions (anterior, right lateral, posterior, and left lateral) were then defined, each consisting of three lateral zones. Shape and GR were compared across 8 segments defined by the 2 longitudinal and 4 lateral regions (Fig. 5).

Statistical shape modeling

SSM was utilized to compare the mean 3D growth patterns between males and females. Our SSM protocol was adapted from previously published methods and was completed using Python and VMTK. SSM begins by using vessel centerlines to standardize each mesh generated by VDM. The meshes are mapped to a common coordinate system with the iliac bifurcation as the origin, the positive x-axis oriented normal to the iliac bifurcation plane, and the positive z-axis pointing from the iliac bifurcation to the centerline point at the lowest renal artery. Each mesh is then scaled to fit within the unit sphere and matched against a common cylindrical template to establish corresponding points among all meshes[64]. A mean mesh is then computed by averaging the coordinates of the corresponding points across all meshes. The mean growth and mean centerline distance are similarly computed by averaging these metrics across the corresponding points of all meshes.

Evaluation of diameter, volume, shape and growth

The Dmax for each CT scan was obtained from clinical radiology reports by trained 3D image analysis technicians. The AAA volume, including the lumen, ILT, and aortic wall, as well as the isolated ILT volume, was obtained manually using 3D Slicer. Tortuosity was defined as the ratio between the aortic centerline length and the straight-line distance between the same two points.

Aneurysm neck Dmax, length, alpha-angles, and beta-angles were collected from the automated segmentations that passed manual checks for accuracy. Aneurysm neck alpha-angles were defined as the angle between the longitudinal axis of the supra-renal aorta and longitudinal axis of the AAA neck while beta-angles were defined as the angle between the longitudinal axis of the AAA neck and AAA sac[65]. The baseline shape (defined as the distance of the aneurysm surface from the centerline) and GR were calculated for each of the eight regions for each individual patient. Sex differences in shape and GR were then compared for each aortic segment.

The average GR and percentage of surface area with growth (>0.1 and >0.2 cm/year) for the AAA and aneurysm necks were collected and compared between the male- and female-shaped models.

Statistical analysis

Patient characteristics are reported as the mean ± SD for continuous variables and as frequencies for categorical variables. Paired Student's *t* test was used to compare differences in baseline shape and GR between male and female mean shape models on an individual basis for each aortic segment. A p value of <0.05 was considered significant for all the statistical tests. Statistical analyses were performed using Stata 14.0 (StataCorp LP, College Station, TX).

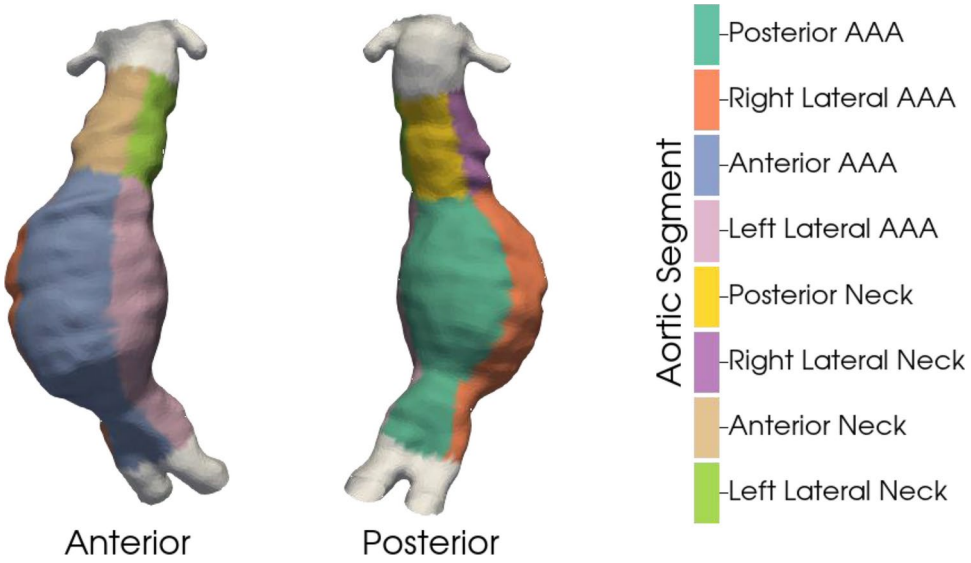

Fig. 5. Aortic regions used for quantitative analysis. Each aorta (derived from VDM) was split into longitudinal zones and lateral zones. Longitudinal zones were defined by setting a value of 1 at the iliac bifurcation and then increasing by a value of 1 for every 5% along the centerline toward the renal arteries (range 1 to 19). Two longitudinal regions were then defined: 1) AAA (1 to 14), 2) aneurysm neck (15 to 19). Lateral zones were defined as 1 for points normal to the plane of the iliac bifurcation and then by an increase of 1 for every 30 degrees circumferentially (range 1 to 12). Four lateral regions were then defined: 1) anterior (1,2,12), 2) right lateral (3,4,5) posterior (6,7,8), and 4) left lateral (9,10,11). Using two longitudinal and four lateral regions, aortic growth can be compared across 8 segments.

Data availability

The datasets generated during and/or analyzed during the current study are available from the corresponding author on reasonable request.

Received: 16 May 2024; Accepted: 4 October 2024
Published online: 16 October 2024

References

1. Kniemeyer, H. W. et al. Treatment of ruptured abdominal aortic aneurysm, a permanent challenge or a waste of resources? Prediction of outcome using a multi-organ-dysfunction score. *Eur. J. Vasc. Endovasc. Surg.* **19**, 190–196 (2000).
2. van der Vliet, J. A. & Boll, A. P. Abdominal aortic aneurysm. *Lancet* **349**, 863–866 (1997).
3. Choksy, S. A., Wilmink, A. B. & Quick, C. R. Ruptured abdominal aortic aneurysm in the Huntingdon district: A 10-year experience. *Ann. R. Coll. Surg. Engl.* **81**, 27–31 (1999).
4. Lederle, F. A. et al. Rupture rate of large abdominal aortic aneurysms in patients refusing or unfit for elective repair. *JAMA* **287**, 2968–2972 (2002).
5. Lederle, F. A. et al. Immediate repair compared with surveillance of small abdominal aortic aneurysms. *N. Engl. J. Med.* **346**, 1437–1444 (2002).
6. Powell, J. T. et al. Final 12-year follow-up of surgery versus surveillance in the UK Small Aneurysm Trial. *Br. J. Surg.* **94**, 702–708 (2007).
7. Parkinson, F. et al. Rupture rates of untreated large abdominal aortic aneurysms in patients unfit for elective repair. *J. Vasc. Surg.* **61**, 1606–1612 (2015).
8. Dryjski, M. et al. The small abdominal aortic aneurysm: The eternal dilemma. *J. Cardiovasc. Surg. (Torino)* **35**, 95–100 (1994).
9. Chaikof, E. L. et al. The Society for Vascular Surgery practice guidelines on the care of patients with an abdominal aortic aneurysm. *J. Vasc. Surg.* **67**, 2-77.e2 (2018).
10. Finol, E. A. & Amon, C. H. Blood flow in abdominal aortic aneurysms: Pulsatile flow hemodynamics. *J. Biomech. Eng.* **123**, 474–484 (2001).
11. Powell, J. T. et al. Systematic review and meta-analysis of growth rates of small abdominal aortic aneurysms. *Br. J. Surg.* **98**, 609–618 (2011).
12. Hua, J. & Mower, W. R. Simple geometric characteristics fail to reliably predict abdominal aortic aneurysm wall stresses. *J. Vasc. Surg.* **34**, 308–315 (2001).
13. Vorp, D. A., Raghavan, M. L. & Webster, M. W. Mechanical wall stress in abdominal aortic aneurysm: Influence of diameter and asymmetry. *J. Vasc. Surg.* **27**, 632–639 (1998).
14. Kontopodis, N. et al. Advances in determining abdominal aortic aneurysm size and growth. *World J. Radiol.* **8**, 148–158 (2016).
15. Kauffmann, C. et al. Measurements and detection of abdominal aortic aneurysm growth: Accuracy and reproducibility of a segmentation software. *Eur. J. Radiol.* **81**, 1688 (2012).
16. Parr, A., Jayaratne, C., Buttner, P. & Golledge, J. Comparison of volume and diameter measurement in assessing small abdominal aortic aneurysm expansion examined using computed tomographic angiography. *Eur. J. Radiol.* **79**, 42–47 (2011).
17. Kontopodis, N. et al. Value of volume measurements in evaluating abdominal aortic aneurysms growth rate and need for surgical treatment. *Eur. J. Radiol.* **83**, 1051–1056 (2014).
18. Olson, S. L. et al. Role of volume in small abdominal aortic aneurysm surveillance. *J. Vasc. Surg.* **75**, 1260-1267.e3 (2022).
19. Zielinski, A. H. et al. One-year volume growth of abdominal aortic aneurysms measured by extended field-of-view ultrasound. *Int. Angiol.* **42**, 80–87 (2023).
20. Siika, A. et al. Three-dimensional growth and biomechanical risk progression of abdominal aortic aneurysms under serial computed tomography assessment. *Sci. Rep.* **13**, 9283 (2023).
21. Cheung, K. et al. Thoracic aortic aneurysm growth: Role of sex and aneurysm etiology. *JAHA* **6**, e003792 (2017).
22. Mofidi, R. et al. Influence of sex on expansion rate of abdominal aortic aneurysms. *Br. J. Surg.* **94**, 310–314 (2007).
23. Forbes, T. L., Lawlor, D. K., DeRose, G. & Harris, K. A. Gender differences in relative dilatation of abdominal aortic aneurysms. *Ann. Vasc. Surg.* **20**, 564–568 (2006).
24. Li, X., Zhao, G., Zhang, J., Duan, Z. & Xin, S. Prevalence and trends of the abdominal aortic aneurysms epidemic in general population—A meta-analysis. *PLoS ONE* **8**, e81260 (2013).
25. Brown, L. C. & Powell, J. T. Risk factors for aneurysm rupture in patients kept under ultrasound surveillance. UK Small Aneurysm Trial Participants. *Ann. Surg.* **230**, 289–296 (1999) (**discussion 296–297**).
26. Brown, P. M., Zelt, D. T. & Sobolev, B. The risk of rupture in untreated aneurysms: The impact of size, gender, and expansion rate. *J. Vasc. Surg.* **37**, 280–284 (2003).
27. Boczar, K. E. et al. Sex differences in thoracic aortic aneurysm growth. *Hypertension* **73**, 190–196 (2019).
28. Boese, A. C. et al. Sex differences in abdominal aortic aneurysms. *Am. J. Physiol. Heart Circ. Physiol.* **314**, H1137–H1152 (2018).
29. Sweet, M. P., Fillinger, M. F., Morrison, T. M. & Abel, D. The influence of gender and aortic aneurysm size on eligibility for endovascular abdominal aortic aneurysm repair. *J. Vasc. Surg.* **54**, 931–937 (2011).
30. Shutze, W. P. et al. Sex as an independent risk factor for long-term survival after endovascular aneurysm repair. *J. Vasc. Surg.* **69**, 1080-1089.e1 (2019).
31. Karthaus, E. G., Tong, T. M. L., Vahl, A., Hamming, J. F., & Dutch Society of Vascular Surgery, the Steering Committee of the Dutch Surgical Aneurysm Audit and the Dutch Institute for Clinical Auditing. Saccular Abdominal Aortic Aneurysms: Patient Characteristics, Clinical Presentation, Treatment, and Outcomes in the Netherlands. *Ann Surg* **270**, 852–858 (2019).
32. Taylor, B. V. & Kalman, P. G. Saccular aortic aneurysms. *Ann. Vasc. Surg.* **13**, 555–559 (1999).
33. Kristmundsson, T., Dias, N., Resch, T. & Sonesson, B. Morphology of small abdominal aortic aneurysms should be considered before continued ultrasound surveillance. *Ann. Vasc. Surg.* **31**, 18–22 (2016).
34. Braet, D. J. et al. Vascular deformation mapping of abdominal aortic aneurysm. *TomographyBold"*>*7*, 189–201 (2021).
35. Burris, N. S., Hoff, B. A., Kazerooni, E. A. & Ross, B. D. Vascular deformation mapping (VDM) of thoracic aortic enlargement in aneurysmal disease and dissection. *Tomography* **3**, 11 (2017).
36. Burris, N. S., Hoff, B. A., Patel, H. J., Kazerooni, E. A. & Ross, B. D. Three-dimensional growth analysis of thoracic aortic aneurysm with vascular deformation mapping. *Circ. Cardiovasc. Imaging* **11**, e008045 (2018).
37. Burris, N. S., Hoff, B. A. & Ross, B. D. Vascular deformation mapping (VDM) of thoracic aortic aneurysm: An application for color 3D printing in aortic disease. *Ann. Transl. Med.* **6**, S123 (2018).
38. Burris, N. S. et al. Vascular deformation mapping for CT surveillance of thoracic aortic aneurysm growth. *Radiology* **302**, 218–225 (2022).
39. Stoecker, J. B., Eddinger, K. C., Pouch, A. M., Vrudhula, A. & Jackson, B. M. Local aortic aneurysm wall expansion measured with automated image analysis. *JVS-Vasc. Sci.* **3**, 48–63 (2022).
40. Ambellan, F., Lamecker, H., von Tycowicz, C. & Zachow, S. Statistical shape models: Understanding and mastering variation in anatomy. *Adv. Exp. Med. Biol.* **1156**, 67–84 (2019).

41. Jolliffe, I. T. & Cadima, J. Principal component analysis: A review and recent developments. *Philos. Trans. A Math. Phys. Eng. Sci.* **374**, 20150202 (2016).
42. Khan, N. et al. Statistical multi-level shape models for scalable modeling of multi-organ anatomies. *Front. Bioeng. Biotechnol.* **11**, 1089113 (2023).
43. Johnson, L. G. & Pawliuk, C. Application of statistical shape modeling to the human hip joint: A scoping review protocol. *JBI Evid. Synth.* **19**, 1211–1221 (2021).
44. IJpma, F. F. A. et al. Feasibility of imaging-based 3-dimensional models to design patient-specific osteosynthesis plates and drilling guides. *JAMA Netw. Open* **4**, e2037519 (2021).
45. Fuessinger, M. A. et al. Virtual reconstruction of bilateral midfacial defects by using statistical shape modeling. *J. Craniomaxillofac. Surg.* **47**, 1054–1059 (2019).
46. Semper-Hogg, W. et al. Virtual reconstruction of midface defects using statistical shape models. *J. Craniomaxillofac. Surg.* **45**, 461–466 (2017).
47. van Veldhuizen, W. A. et al. A statistical shape model of the morphological variation of the infrarenal abdominal aortic aneurysm neck. *J. Clin. Med.* **11**, 1687 (2022).
48. Vande Geest, J. P. et al. Gender-related differences in the tensile strength of abdominal aortic aneurysm. *Ann. N. Y. Acad. Sci.* **1085**, 400–402 (2006).
49. Szilagyi, D. E., Smith, R. F., DeRusso, F. J., Elliott, J. P. & Sherrin, F. W. Contribution of abdominal aortic aneurysmectomy to prolongation of life. *Ann. Surg.* **164**, 678–699 (1966).
50. Stringfellow, M. M., Lawrence, P. F. & Stringfellow, R. G. The influence of aorta-aneurysm geometry upon stress in the aneurysm wall. *J. Surg. Res.* **42**, 425–433 (1987).
51. Fillinger, M. F. et al. Anatomic characteristics of ruptured abdominal aortic aneurysm on conventional CT scans: Implications for rupture risk. *J. Vasc. Surg.* **39**, 1243–1252 (2004).
52. Nathan, D. P. et al. Increased wall stress of saccular versus fusiform aneurysms of the descending thoracic aorta. *Ann. Vasc. Surg. Bold"*>*25*, 1129–1137 (2011).
53. Teng, B., Zhou, Z., Zhao, Y. & Wang, Z. Combined curvature and wall shear stress analysis of abdominal aortic aneurysm: An analysis of rupture risk factors. *Cardiovasc. Intervent. Radiol.* **45**, 752–760 (2022).
54. Chandrashekar, A. et al. Prediction of abdominal aortic aneurysm growth using geometric assessment of computerized tomography images acquired during the aneurysm surveillance period. *Ann. Surg.* **277**, e175–e183 (2023).
55. de Galarreta, S. R., Cazón, A., Antón, R. & Finol, E. A. The relationship between surface curvature and abdominal aortic aneurysm wall stress. *J. Biomech. Eng.* **139**, 081006 (2017).
56. Cayne, N. S. et al. Variability of maximal aortic aneurysm diameter measurements on CT scan: Significance and methods to minimize. *J. Vasc. Surg.* **39**, 811–815 (2004).
57. Lederle, F. A. et al. Variability in measurement of abdominal aortic aneurysms. Abdominal aortic aneurysm detection and management veterans administration cooperative study group. *J. Vasc. Surg.* **21**, 945–952 (1995).
58. Klein, S., Staring, M. & Pluim, J. P. W. Evaluation of optimization methods for nonrigid medical image registration using mutual information and B-splines. *IEEE Trans. Image Process.* **16**, 2879–2890 (2007).
59. RESCAN Collaborators *et al.* Surveillance intervals for small abdominal aortic aneurysms: a meta-analysis. *JAMA* **309**, 806–813 (2013).
60. Klein, S., Staring, M., Murphy, K., Viergever, M. A. & Pluim, J. P. W. elastix: A toolbox for intensity-based medical image registration. *IEEE Trans. Med Imaging* **29**, 196–205 (2010).
61. Staring, M., Klein, S. & Pluim, J. P. W. A rigidity penalty term for nonrigid registration. *Med. Phys.* **34**, 4098–4108 (2007).
62. Antiga, L. et al. An image-based modeling framework for patient-specific computational hemodynamics. *Med. Biol. Eng. Comput.* **46**, 1097–1112 (2008).
63. Piccinelli, M., Veneziani, A., Steinman, D. A., Remuzzi, A. & Antiga, L. A framework for geometric analysis of vascular structures: Application to cerebral aneurysms. *IEEE Trans. Med. Imaging* **28**, 1141–1155 (2009).
64. Heimann, T. & Meinzer, H.-P. Statistical shape models for 3D medical image segmentation: A review. *Med. Image Anal.* **13**, 543–563 (2009).
65. van Keulen, J. W., Moll, F. L., Tolenaar, J. L., Verhagen, H. J. M. & van Herwaarden, J. A. Validation of a new standardized method to measure proximal aneurysm neck angulation. *J. Vasc. Surg.* **51**, 821–828 (2010).

Acknowledgements

We acknowledge the University of Michigan Medical School Research Data Warehouse and Data Direct for providing data aggregation, management, and distribution services in support of the research in the present report.

Author contributions

Conception and Design: DJB, CAF, JLE, NSB Obtaining Funding: JLE, NSB Data Collection: DJB, LD, GS, NG, AA Data Analysis and Interpretation: DJB, TJB, LD, GS, CAF, JLE, NSB Statistical Analysis: DJB Manuscript Writing: DJB, TJB, LD, CAF, JE, NSB Critical Revision: DJB, TJB, LD, GS, NG, AA, CAF, JLE, NSB Approval of Manuscript: DJB, TJB, LD, GS, NG, AA, CAF, JLE, NSB.

Funding

Jonathan L. Eliason: Baiardi Family Foundation, Harbor Springs, Michigan. Nicholas S. Burris: National Institutes of Health (R44HL145953).

Competing interests

The authors declare no competing interests.

Additional information

Supplementary Information The online version contains supplementary material available at https://doi.org/10.1038/s41598-024-75334-z.

Correspondence and requests for materials should be addressed to D.J.B.